Large moments in bcc $Fe_XCo_YMn_Z$ ternary alloy thin films

R. J. Snow, H. Bhatkar, A. T. N'Diaye, E. Arenholz, and Y. U. Idzerda

Citation: Appl. Phys. Lett. **112**, 072403 (2018); doi: 10.1063/1.5006347
View online: https://doi.org/10.1063/1.5006347
View Table of Contents: http://aip.scitation.org/toc/apl/112/7
Published by the American Institute of Physics

Large moments in bcc $Fe_xCo_yMn_z$ ternary alloy thin films

R. J. Snow,[1] H. Bhatkar,[1] A. T. N'Diaye,[2] E. Arenholz,[2] and Y. U. Idzerda[1,a)]
[1]*Department of Physics; Montana State University, Bozeman, Montana 59715, USA*
[2]*Advanced Light Source, Lawrence Berkeley Nat. Labs, Berkeley, California 94720, USA*

(Received 25 September 2017; accepted 25 January 2018; published online 13 February 2018)

The elemental magnetic moments and the average atomic moment of 10–20 nm thick single crystal bcc (bct) $Fe_xCo_yMn_z$ films deposited on MgO(001) have been determined as a function of a broad range of compositions. Thin film epitaxy stabilized the bcc structure for 80% of the available ternary compositional space compared to only a 23% stability region for the bulk. The films that display ferromagnetism represent 60% of the available compositional possibilities compared to 25% for the bulk. A maximum average atomic moment of $3.25 \pm 0.3\ \mu_B$/atom was observed for a bcc $Fe_9Co_{62}Mn_{29}$ film (well above the limit of the Slater-Pauling binary alloy curve of $2.45\ \mu_B$/atom). The $Fe_xCo_yMn_z$ ternary alloys that exhibit high moments can only be synthesized as ultrathin films since the bcc structure is not stable in the bulk for those compositions. *Published by AIP Publishing.*
https://doi.org/10.1063/1.5006347

Large magnetic moment materials are essential components in a variety of technologies but are increasingly important and in many cases the major limiting factor in information processing and data storage.[1,2] For ultrathin film application, large moments are particularly important in high-density memory applications,[3] spin torque hierarchies,[4] BH-energy product device structures,[5] the control of spinor applications in nanoscale non-collinear magnets,[6] and establishing enhanced electron spin-polarizations at the Fermi level.[7] Increasing the average atomic moment of these films can significantly improve their performance. In addition, epitaxial ultrathin films offer opportunities in spin-transport performance control through the modification of magnetic properties due to the reduced dimensionality and structural distortions created by film/lattice mismatches. One important prospect is that energies associated with epitaxial substrate/overlayer lattice matching of single crystal films often extend the range of structural stabilities beyond that available in the bulk, including the stabilization of film structures not present in the bulk phase diagram.[8]

The establishment of high moment alloy films typically includes the incorporation of transition metal elements that have large moments. The magnetic moments for transition metal binary alloys are conventionally displayed in the form of a plot of the saturation magnetization density (M_S) or moment per atom as a function of the number of electrons.[9] As implemented by Slater[10] and Pauling,[11] the Slater-Pauling (SP) curve is displayed in the form of a triangle-shaped graph depicting a linear variation (first increasing and then decreasing) of the mean atomic moment in Bohr magnetons/atom (μ_B/atom) regardless of the atom type. The maximum achievable moment is $2.45\ \mu_B$/atom at an electron number of 26.3 for a bcc $Fe_{70}Co_{30}$ alloy (often referred to as the Slater-Pauling limit).[12–14] Improved insight into trends in binary alloy magnetic behavior can be found using a generalized SP formalism[15] which introduces the concepts of magnetic valence[16] implicit in the original SP formulation.

A potential avenue to larger moments is the addition of Mn to the binary bcc FeCo system. Bulk $Fe_xCo_yMn_z$ is quite complex.[17–22] It exhibits strain induced bcc-fcc Bain transitions,[21,23] resulting in a rich structural and magnetic phase diagram but only a limited region where the bulk structure is bcc and ferromagnetic.[18] By synthesizing the ternary bcc $Fe_xCo_yMn_z$ alloy in thin film form, the bcc structure should be maintainable over a larger compositional range than the bulk. Single crystal, bcc films of Fe, Co, Fe_xCo_{1-x}, $Fe_{1-z}Mn_z$, and Co_yMn_{1-y} have already been stabilized on MgO(001) and GaAs(001) substrates.[8,24–28] It should be noted that the bcc Co is synthesized as a forced structure where interfacial energies maintain the bcc structure but only to a finite thickness.[29,30] (Metastable films have no thickness limitation in principle.) The bcc FeCo has been stabilized for the entire composition range, remaining ferromagnetic.[31] The bcc $Fe_{1-z}Mn_z$ growth on MgO(001) is stable in thin film form for $0.65 \leq x \leq 1$, while its bulk stability range is $0.88 \leq x \leq 1$.[32] In the bulk, Co_yMn_{1-y} is stable only as an fcc or hcp structure. The bulk moment is observed to linearly reduce from a starting value of $1.5\ \mu_B$/atom for pure hcp Co and vanishing at $Co_{75}Mn_{25}$.[9,33,34] In contrast, thin films of the Co_yMn_{1-y} alloys are shown to be stable as bcc (bct) structures from $1 < y < 0.3$, and the average moment is seen to increase with Mn addition, beginning at $1.65\ \mu_B$/atom for pure Co to a concentration of $Co_{76}Mn_{24}$ after which the moment is observed to reduce linearly with the increasing Mn content and collapse at $Co_{35}Mn_{65}$.

The $Fe_xCo_yMn_z$ films are synthesized by molecular beam epitaxy (MBE) on 0.5 mm thick polished MgO(001) substrates (from MTI corporation) using separate Knudsen cell sources. The MgO substrates are sonicated for 5 min in acetone and then for 5 min in methanol (the final deionized (DI) water rinse is avoided due to the hygroscopic nature of MgO). The substrates are mounted using indium solder to a 3 in. diameter molybdenum sample puck and placed into the vacuum chamber via a load-lock antechamber. The samples are vacuum annealed at 850 °C for a minimum of 15 min prior to transfer into the MBE growth chamber. An insufficient heat-anneal or exposure to water vapor (due to improper substrate

a)Author to whom correspondence should be addressed: Idzerda@montana.edu

storage) resulted in oxidation of the film at the MgO interface due to absorbed water which diffuses to the interface.[27]

The films are grown at a base pressure of $\sim 1 \times 10^{-9}$ Torr with the substrate held at 160 °C. The film composition is controlled by the Knudsen cell flux rates set by cell temperatures and calibrated by vibrating sample magnetometry (VSM). Substrates were cooled below 100 °C prior to deposition of an amorphous aluminum capping layer of thickness 3.5 nm to minimize interlayer mixing. Sample compositions are determined using integrated X-ray absorption spectroscopy (XAS) of the L_3-edge of the constituent components and used to verify relative flux rates.

The structural identification is monitored by Reflection High-Energy Electron Diffraction (RHEED). Due to the lattice mismatch of the $Fe_xCo_yMn_z$ films with the underlying substrate, the films are most likely tetragonally distorted from the bcc configuration to form a bct film. Since MgO is an insulating material, substrate charging can distort the RHEED diffraction pattern, resulting in broad fuzzy lines. Still, $Fe_xCo_yMn_z$ generates a strong RHEED pattern consistent with a bcc surface net rotated 45° with respect to the underlying MgO (similar to what has been observed for bcc Fe,[24] Co,[8] FeM,[32] and CoMn[27] films).

Sample compositions are targeted from our calibrated flux rates and determined from the area (after removal of the linear pre-edge background) of the XAS L_3 peak for Fe, Co, and Mn (as has been performed elsewhere[27,32]). In addition to the compositional determinations, the individual atomic moments and the total average moment can be determined by X-ray magnetic circular dichroism (XMCD). The XMCD and XAS measurements are performed at Beamline 6.3.1.1 of the Advanced Light Source of Lawrence Berkeley National Laboratories with some measurements made at Beamline 4.0.2. The compositional and elemental moment data are collected sequentially at the same position on the sample. The XAS is acquired in the total electron yield mode (sample current), while the photon energy is scanned through the Fe, Co, and Mn $L_{2,3}$-edges using linearly polarized soft-x-rays. The XMCD measurements of the same L-edges are acquired using elliptically polarized light with the soft-x-ray incident at 60° from normal incidence while the 0.1–0.5 T applied magnetic field is reversed (equivalently, the X-ray polarization could also be reversed). Since the field is coaxial with the photon propagation direction, care must be taken to ensure that the moment remains in the sample plane by using the minimum magnetic field strength, which results in a total moment reversal. This was verified by comparing XMCD values with those acquired using the vector magnetic field capability at beamline 4.0.2 where the magnetic field can be applied in the sample plane.

Any variation in the XMCD intensity represents a change in the elemental moment. For accurate moment values, the moment extraction from the XMCD spectra is calibrated using a pure bcc Fe film with a known moment of 2.2 μ_B/atom and a pure bcc Co film with a theoretical value of 1.65 μ_B/atom.[35] We have used the theoretical value since the experimentally determined values of the Co moment vary from 1.5 to 1.7 μ_B/atom.[8,36] For the Mn moment calibration, we use a value of 3.0 μ_B/atom for low Mn concentrations that we determine from LDA calculations which is in agreement with other theoretical values.[37] The total average moment is the sum of the average individual moments weighted by the compositional fraction of the film (as determined by XAS).

The average atomic moment as a function of composition of a ternary alloy such as $Fe_xCo_yMn_z$ is often displayed in a triangular composition diagram where the average atomic moment is represented by a color and the 3 edges of the triangle represent each of the three composition variables (x, y, z). The central image in Fig. 1 displays the average atomic moment (in μ_B/atom, independent of the type of atom) as a function of alloy composition for bcc (bct) $Fe_xCo_yMn_z$ films. This image is created using a 3rd-degree polynomial spline interpolation of a sparse dataset consisting of 48 ternary compositions, represented by the green crosses, and the binary alloy data associated with the triangle sides. The vertical dashed lines represent the constant electron number for comparison to the Slater-Pauling curve and vary from 27.0 to 25.0 going to the right. The vertices of the triangle represent pure elements (for comparative purposes, the vertex assignments follow the study by Matsui[18]), with the lower left vertex representing Co, the lower right vertex representing Mn, and the apex of the triangle representing Fe. The top color bar relates the color to the moment value, indicating a maximum measured average atomic moment of 3.25 ± 0.3 μ_B/atom (compared to the Slater-Puling limit value of 2.4 μ_B/atom).

Adjacent to each edge of the triangle are graphs of the average atomic moment for the binary alloys for bulk and/or thin films (also grown on MgO). The figure along the left triangle leg corresponds to the bulk bcc Fe_xCo_{1-x} ($z = 0$) from the study by Weiss[38] and includes the Slater-Pauling limit value of 2.4 μ_B/atom at the $Fe_{70}Co_{30}$ composition point (corresponding to an electron number of 26.3). Thin film MBE growth has been shown to stabilize the bcc structure to pure Co for deposition on GaAs(001)[8,36] and MgO(001)[28] surfaces. The figure along the right triangle leg corresponds to

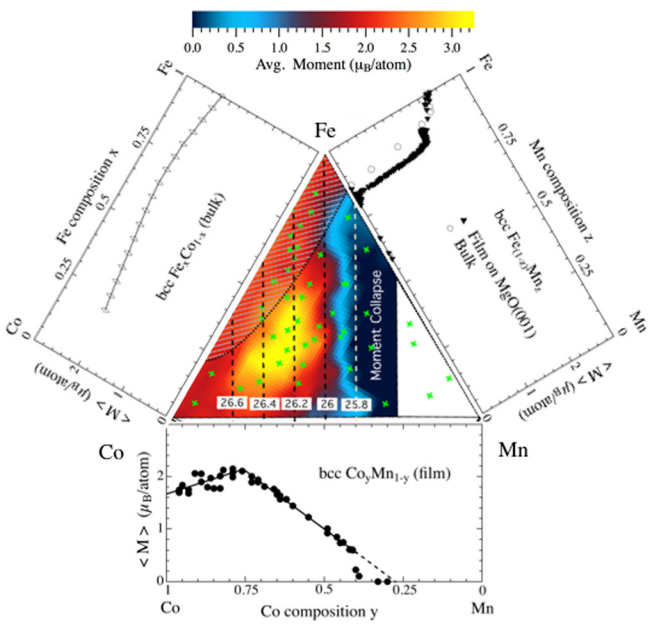

FIG. 1. The average total atomic moment (independent of atom type) for 10 nm $Fe_xCo_yMn_z$ films on MgO(001) as a function of composition. The green crosses represent the measured data points.

both the bulk and thin film average moment values for bcc $Fe_{1-z}Mn_z$ ($y = 0$).[26,32] The figure along the bottom of the triangle corresponds to the films of bcc Co_yMn_{1-y} ($x = 0$)[27] (note that the Co composition decreases to the right). The data points of these three binary alloy graphs represent the moment values along the edges of the ternary alloy triangle. A point of interest is that although Mn is typically found to be anti-aligned to the host in transition metal alloys, we find that in CoMn, Mn is aligned to Co[27] and that in FeMn, either the Mn moment is very small or the Mn spin is frustrated.[32] In the FeCoMn system, both spin configurations occur for the Mn, while Fe and Co are always aligned to each other. In the region of high total moment, Mn is always aligned with the other two elements.

A major finding of this work is that the bcc phase can be stabilized to 80% of the available ternary compositional space. The region of bulk stability for the α-phase (bcc) is from the study by Matsui[18] and is shown by the diagonal striped area beginning in the apex of the triangle, down most of the left side of the triangle, and bound by the curved dashed line. The bcc (bct) stability region for the epitaxial films (as determined from the RHEED data) is the regions with color. The small white area at the bottom right represents the region that could not be stabilized as bcc (bct) and is exclusively in the region of high Mn compositions, corresponding fairly well to the onset of the β-phase in the bulk phase diagram.[18] The line of instability is mainly inferred from the binary alloy data with a few ternary growths used for confirmation. Note that the regions of high average moment (yellow) are for compositions that are not stable in the bulk.

In addition to the compositional labels for the triangular figure, the lines of constant electron number show that there are a large range of compositions with the same electron number for the $Fe_xCo_yMn_z$ alloys that have very different moment values. Interestingly, the thin film bcc ternary system is ferromagnetic above an electron number of 25.85 below which the moment collapses, most likely due to the onset of spin frustration or anti-ferromagnetism. The moment collapse is separate from the bcc instability which occurs near the electron number of 25.55. The largest average atomic moment is found to be $3.25 \pm 0.3\ \mu_B$/atom for an $Fe_{09}Co_{62}Mn_{29}$ film which corresponds to an electron number of 26.33 ± 0.08, slightly higher than the Slater-Pauling value for binary alloys.

To estimate the magnetization density of these films, we measured the total film moment by vibrating sample magnetometry (VSM) and the thickness by cross-sectional TEM measurements on a $Fe_{09}Co_{62}Mn_{29}$ film grown on a $5.0 \pm 0.1\ \text{mm} \times 5.0 \pm 0.1\ \text{mm}$ MgO(100) substrate. The total film moment was measured to be $3.14 \pm 0.04 \times 10^{-7}\ \text{A m}^2$, and the thickness was determined to be $5.8 \pm 0.5\ \text{nm}$. Assuming that the film area is the same as the substrate surface area (which ignores oxidation at the sample edges), the magnetization density for this composition is found to be $2.165 \pm 0.19 \times 10^6$ A/m (or 2.72 ± 0.24 T) which is in excess of the Slater Pauling limit.

The informationally dense data of the average atomic moment as a function of composition graph can be redisplayed in useful ways. For a direct comparison to the Slater-Pauling curve, these data can be displayed as a function of electron number. Figure 2 replaces the 3D color plot with a more traditional line plot of the same average atomic moment data but plotted as a function of electron number for the range of electron numbers where the bcc phase is stabilized (25.5 to 27.0, but now increasing to the right instead of decreasing). The $Fe_xCo_yMn_z$ data are the filled circles. The bcc $Fe_{1-z}Mn_z$ and the Co_yMn_{1-y} films are the open red diamonds and open blue squares, respectively. The bulk bcc FeCo data are shown as the dashed line. Also included here are the data for bulk FeV (solid line).

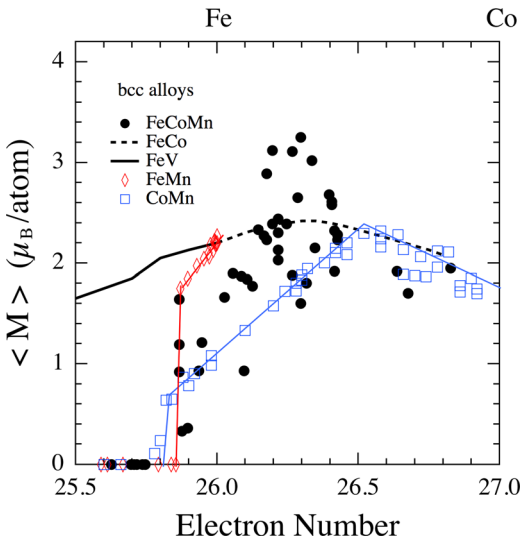

FIG. 2. Average total atomic moment as a function of electron number for FeCoMn films (black dots) and various binary alloys.

While the binary alloy moment data are single valued, the ternary data are multi-valued demonstrating that the Slater-Pauling formalisms lack utility for this ternary system. Moments above the Slater-Pauling limit (peak in the FeCo line) are limited to electron numbers from 26.2 to 26.4. Furthermore, the moment collapse occurs at an electron number of 25.85 ± 0.05 for all three Mn-based alloys. The FeV alloy remains ferromagnetic well below this electron number, suggesting that Mn is intrinsic to the moment collapse.

Having determined that the average atomic moment as a function of electron number is multi-valued, it may be informative to compare the elemental atomic moment as a function of composition for a constant electron number. Figure 3 displays the average atomic moment as a function of the Fe atomic concentration (black line and filled circles), Co atomic concentration (blue line and empty diamonds), and Mn concentration (red line and empty squares) for films with an electron number of 26.2 ± 0.05 electrons. The elemental atomic concentrations are obtained from the XAS measurements (used for the composition determination), and the elemental moments are obtained from the MCD measurements to arrive at the average atomic moment. This restricted sample set includes 12 ternary alloys and also includes the data for the $x = 0$ point ($Co_{60}Mn_{40}$ binary alloy). Three data points, one for each elemental composition, are generated for each average atomic moment value.

Maintaining a constant 26.2 electron number restricts the available ranges for each element concentration to $0 < z < 0.4$ for Mn, $0.2 < y < 0.6$ for Co, and $0 < x < 0.8$ for Fe. Fitting a linear least-squares fit to each elemental dataset

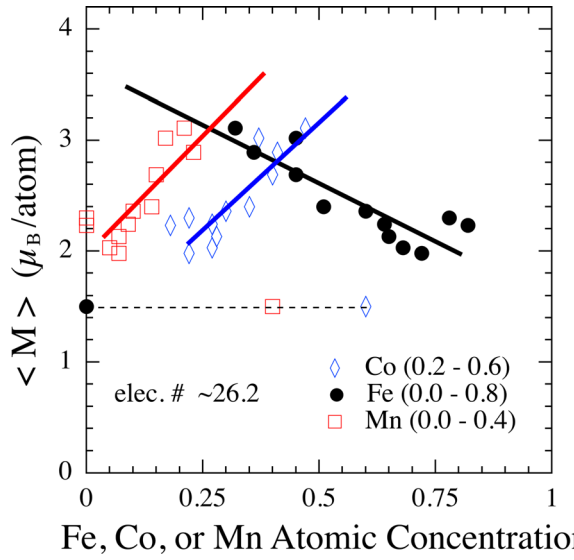

FIG. 3. Average total atomic moment as a function of Mn (red squares), Co (blue diamonds), and Fe (black circles) for FeCoMn films with an electron number of 26.2 ± 0.05.

(excluding the $Co_{60}Mn_{40}$ data point) results in three trend lines which are displayed as solid lines. The trends consistently show that the atomic moment is seen to increase with the decreasing Fe content. Still, as the Fe content is further reduced, the average total moment must subsequently decline to be in agreement with the low measured moment value of $Co_{60}Mn_{40}$ (occurring at $x = 0$), indicated by the horizontal dashed line at 1.5 μ_B/atom.

Further improvements in the total moment may be found by investigating the lower Fe content and nearby electron numbers greater than 26.33. Also, the addition of large moment Cr as either bcc FeCoCr or bcc FeCoMnCr may further enhance moments and further stabilize the bcc structure.

We have synthesized and determined both the elemental net magnetic moments and the average atomic moment (independent of atom type) of bcc $Fe_xCo_yMn_z$/MgO(100) thin films for a large range of compositions. Due to registry with the underlying substrate, the bcc (bct) structure is stable for nearly 80% of available compositional space, compared to only ~20% for bulk alloys. Within that region of structural stability, the region that displays ferromagnetism has been increased to 60% of available compositional possibilities compared to ~25% for the bulk, a number that includes both the entire bulk bcc structural range and the (~5%) hcp phase of Co. The maximum average moment is found to be 3.25 ± 0.3 μ_B/atom for an $Fe_{10}Co_{60}Mn_{30}$ film, well in excess of the Slater-Pauling limit value of 2.45 μ_B/atom for an $Fe_{75}Co_{25}$ film. The compositions with large moments are inaccessible in the bulk.

The Advanced Light Source was supported by the Director, Office of Science, Office of Basic Energy Sciences, of the U.S. Department of Energy under Contract No. DE-AC02-05CH11231.

[1]G. Scheunert, O. Heinonen, R. Hardeman, A. Lapicki, M. Gubbins, and R. M. Bowman, Appl. Phys. Rev. **3**(1), 011301 (2016).
[2]R. Skomski, P. Manchanda, P. Kumar, B. Balamurugan, A. Kashyap, and D. J. Sellmyer, IEEE Trans. Magn. **49**(7), 3215–3220 (2013).
[3]Y. Shiroishi, K. Fukuda, I. Tagawa, H. Iwasaki, S. Takenoiri, H. Tanaka, H. Mutoh, and N. Yoshikawa, IEEE Trans. Magn. **45**(10), 3816–3822 (2009).
[4]D. C. Ralph and M. D. Stiles, J. Magn. Magn. Mater. **320**(7), 1190–1216 (2008).
[5]E. E. Fullerton, J. S. Jiang, M. Grimsditch, C. H. Sowers, and S. D. Bader, Phys. Rev. B **58**(18), 12193–12200 (1998).
[6]J. A. Fischer, L. M. Sandratskii, S.-H. Phark, S. Ouazi, A. A. Pasa, D. Sander, and S. S. P. Parkin, Nat. Commun. **7**, 13000 (2016).
[7]I. I. Mazin, Phys. Rev. Lett. **83**(7), 1427–1430 (1999).
[8]G. A. Prinz, Phys. Rev. Lett. **54**(10), 1051–1054 (1985).
[9]R. M. Bozorth, *Ferromagnetism* (D. Van Nostrand Company, New York, 1951).
[10]J. C. Slater, J. Appl. Phys. **8**, 385 (1937).
[11]L. Pauling, Phys. Rev. **54**, 899 (1938).
[12]C. Binns, K. N. Trohidou, J. Bansmann, S. H. Baker, J. A. Blackman, J. P. Bucher, D. Kechrakos, A. Kleibert, S. Louch, K. H. Meiwes-Broer, G. M. Pastor, A. Perez, and Y. Xie, J. Phys. D: Appl. Phys. **38**(22), R357 (2005).
[13]J. M. D. Coey, *Magnetism and Magnetic Materials* (Cambridge University Press, Cambridge, UK, 2012).
[14]P. H. Dederichs, R. Zeller, H. Akai, and H. Ebert, J. Magn. Magn. Mater. **100**(1), 241–260 (1991).
[15]A. R. Williams, V. L. Moruzzi, A. P. Malozemoff, and K. Terakura, IEEE Trans. Magn. **19**(5), 1983–1988 (1983).
[16]A. R. Williams, A. P. Malozemoff, V. L. Moruzzi, and M. Matsui, J. Appl. Phys. **55**(6), 2353–2355 (1984).
[17]P. Marinelli, M. Sade, and A. Fernández Guillermet, Scr. Mater. **46**(11), 805–810 (2002).
[18]M. Matsui, K. Sato, and K. Adachi, J. Phys. Soc. Jpn. **35**(2), 419–425 (1973).
[19]W. Huang, Calphad **14**(1), 11–22 (1990).
[20]E. F. Wasserman, "Chapter 3 Invar: Moment-volume instabilities in transition metals and alloys," in *Handbook of Ferromagnetic Materials* (Elsevier, 1990), p. 237–322.
[21]U. Sarı and T. Kırındı, Mater. Chem. Phys. **130**(1), 738–742 (2011).
[22]M. Sicot, S. Andrieu, F. Bertran, and F. Fortuna, Mater. Sci. Eng.: B **126**(2), 151–154 (2006).
[23]R. Skomski, V. Sharma, B. Balamurugan, J. Shield, A. Kashyap, and D. Sellmyer, Proc. REPM **10**, 55–60 (2010).
[24]G. A. Prinz and J. J. Krebs, Appl. Phys. Lett. **39**(5), 397–399 (1981).
[25]Y. Y. Huang, C. Liu, and G. P. Felcher, Phys. Rev. B **47**(1), 183–189 (1993).
[26]Y. U. Idzerda, H. Bhatkar, and E. Arenholz, J. Appl. Phys. **117**(17), 17A721 (2015).
[27]R. J. Snow, H. Bhatkar, A. T. N'Diaye, E. Arenholz, and Y. U. Idzerda, J. Magn. Magn. Mater. **419**, 490 (2016).
[28]M. Sicot, S. Andrieu, F. Bertran, and F. Fortuna, Phys. Rev. B **72**(14), 144414 (2005).
[29]A. Y. Liu and D. J. Singh, Phys. Rev. B **47**(14), 8515–8519 (1993).
[30]A. Y. Liu and D. J. Singh, J. Appl. Phys. **73**(10), 6189–6191 (1993).
[31]C. J. Gutierrez, J. J. Krebs, and G. A. Prinz, Appl. Phys. Lett. **61**(20), 2476–2478 (1992).
[32]H. Bhatkar, R. J. Snow, E. Arenholz, and Y. U. Idzerda, J. Magn. Magn. Mater. **423**, 46 (2017).
[33]S. Sadron, Ann. Phvs. **10**(17), 371 (1932).
[34]J. W. Cable and Y. Tsunoda, J. Magn. Magn. Mater. **140–144**, 93–94 (1995).
[35]D. Wu, G. L. Liu, C. Jing, Y. Z. Wu, D. Loison, G. S. Dong, X. F. Jin, and D.-S. Wang, Phys. Rev. B **63**(21), 214403 (2001).
[36]Y. Z. Wu, H. F. Ding, C. Jing, D. Wu, G. L. Liu, V. Gordon, G. S. Dong, X. F. Jin, S. Zhu, and K. Sun, Phys. Rev. B **57**(19), 11935–11938 (1998).
[37]J. I. Lee, C. L. Fu, and A. J. Freeman, J. Magn. Magn. Mater. **62**(1), 93–100 (1986).
[38]P. Weiss and R. Forrer, Ann. Phys. **10**(12), 279 (1929).